Proton capture to continuum states of ^{209}Bi

A. Likar, M. Lipoglavšek, M. Vencelj, and T. Vidmar
J. Stefan Institute, 1000 Ljubljana, Slovenia

R. A. Bark, E. Gueorguieva, F. Komati, J. J. Lawrie, S. M. Maliage,
S. M. Mullins, S. H. T. Murray, and T. M. Ramashidzha
iThemba LABS, 7129 Somerset West, South Africa
(Received 20 December 2005; published 20 April 2006)

High resolution spectra from fast proton radiative capture in ^{208}Pb are presented for three energies of the incident protons: 14.8, 15.7, and 16.9 MeV. The collected spectra were analyzed with emphasis on the region of capture to unbound states in order to search for possible structure and to study the competition between two basically different phenomena: the statistical process versus the fluctuation effects in radiative capture to unbound final states. In the energy region of incoming protons considered in our experiment, the statistical processes modeled with a Hauser-Feshbach calculation dominate. The spectra of primary γ rays, coincident with the low energy one from the decay of the $f_{7/2}$ single-particle state, show a prominent structure which is predominantly of $g_{9/2}$ character. The calculations of continuum spectra based on the extended direct-semidirect model and the Hauser-Feshbach statistical approach successfully reproduce the experimental data.

DOI: 10.1103/PhysRevC.73.044609 PACS number(s): 25.40.Lw, 23.20.Lv, 24.30.Cz, 27.80.+w

I. INTRODUCTION

In our previous works [1,2], we studied proton radiative capture in ^{208}Pb using the high resolution Ge detectors of the AFRODITE detector array at iThemba LABS. The collected spectra show prominent, well-separated peaks corresponding to proton capture into different single-particle states of the final nucleus ^{209}Bi. These high resolution spectra offer a possibility to search for any structure in the unbound region as well. Indeed, the capture to the $p_{1/2}$ state shows a clearly observable peak, although this state is slightly unbound. The spectra were collected at three different incident proton energies in order to uncover eventual structure in the unbound region. With increasing proton energy, any such structure should appear at a higher energy in the γ-ray spectrum in the same manner as the lines corresponding to capture to the bound states do. Since the density of states rapidly increases in the unbound region, the existence of well-isolated states is not expected. The proton stripping experiments [3] indeed show fluctuating spectra in the continuum region in sharp contrast with the bound region, where the prominent peaks are easily identified as single-particle states with high spectroscopic factors. Broad structures in the region of excitation energies between 4 and 13 MeV were identified as $i_{11/2}$ and $j_{15/2}$ single-particle orbitals. Due to the enhanced sensitivity of the chosen (α, T) reaction to high angular momentum transfer, the $g_{9/2}$ strength was obviously overlooked. Since our coincidence spectra are not sensitive to $i_{11/2}$ and $j_{15/2}$ orbitals, we offer here a complementary view to the high spin proton outer subshells in ^{209}Bi.

In [4], the direct-semidirect (DSD) model, originating from Ref. [5], was extended to treat the fast nucleon capture to virtual single-particle unbound states, which spread into the compound nucleus states after the capture. In the test case of proton capture in ^{89}Y at the proton energy of 19.6 MeV, the authors convincingly show that the experimental data are well reproduced by considering only statistical and direct-semidirect processes without any need for additional reaction mechanisms. The experiment was designed to clearly show the need for DSD contribution to unbound states. Namely, for the chosen target nucleus and selected proton energy, the statistical cross section at excitation energies of the final nucleus just above the bound region is two orders of magnitude below the experimental one. In our case, the difference is not as drastic, indicating a much smaller contribution from the DSD process. The calculations with the extended DSD model indeed show relatively small contribution of the DSD capture mechanism compared to the statistical contribution. This is mainly due to the distribution of single-particle strengths close to the energy threshold separating the bound and unbound single-particle states. Because of experimental limitations, we were not able to extend the proton energy into the region where a pure unbound DSD contribution would be dominant. On the other hand, this is of no particular interest to us, since from [4] the importance of the DSD contribution is evident and so is the ability of the theory to correctly predict the magnitude of the cross section. We were able to reproduce the distribution of the $2g_{9/2}$ single-proton strength using the extended DSD model.

II. EXPERIMENT

The experiment was performed at iThemba LABS using proton beams from the separated sector cyclotron [6]. The measurement was performed at nine different beam energies, but we report here only results for the highest three, namely, 16.9, 15.7, and 14.8 MeV. The target consisted of an enriched ^{208}Pb foil with a thickness of 1 mg/cm^2 mounted on a 5 μg/cm^2 thick carbon backing. The average beam intensity was 40 nA, and about 30 h of beam time were used for each beam energy. High energy γ rays following proton capture

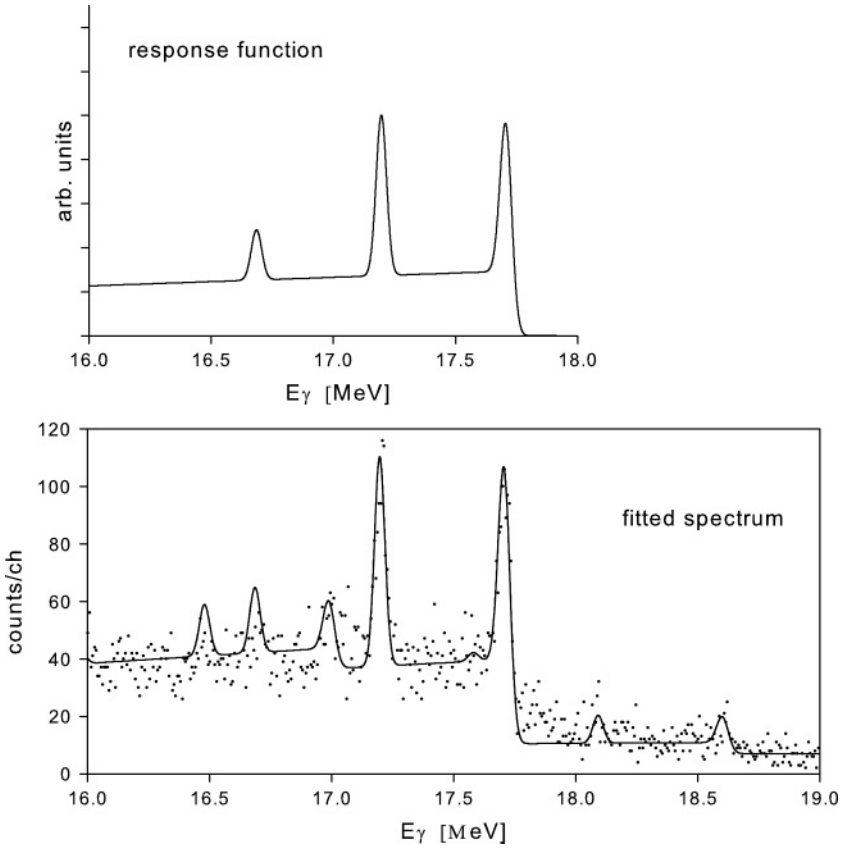

FIG. 1. Elements of response function used to analyze the spectrum at the proton energy of 16.9 MeV. Annotated features correspond to the full energy peak (F), first (E1) and second (E2) escape peaks, and the Compton continuum (Cc).

were detected with the AFRODITE germanium detector array [7], which consisted of eight Ge clover detectors surrounded by the bismuth germanate anti-Compton shields. Each clover detector consists of four tapered Ge crystals packed in a common cryostat [8]. For our experiment, four clover detectors were placed at a 90° polar angle and four at a 135° angle with respect to the beam axis. Standard pulse processing electronics were used, and data were stored on magnetic tapes in LIST mode. Events were accepted if at least one of the 32 Ge crystals gave an energy signal higher than about 3.2 MeV. Signals from all four crystals in a clover detector were added for each event during the data analysis. The beam current was monitored with a Faraday cup and integrated for each run.

To accurately analyze the spectra, the response function of the spectrometer should be known in considerable detail. This requires knowledge of not only the efficiency curve, but also the entire shape of the response curve including the Compton tail and the first and second escape peaks. Monte Carlo simulations using the GEANT3 package [9] gave us some indication of the shape of the response function. The high energy part of the final spectra showing prominent peaks due to capture to the bound states were reproduced using Gaussian functions of different heights, widths, and positions, representing the full energy peak and escape peaks, and a linear function with a proper cutoff shape for the part of the detector response due to Compton scattering (see Fig. 1). The parameters of the curves were adjusted to fit the high energy part of the spectrum. Figures showing the spectra with the proper response function give an impression of the quality of such a fit. The pronounced contaminant carbon lines in the case of capture of 16.9 MeV protons indicate that the final spectra are consistent with the adopted response function in a wide energy region and that the parameters are not strongly energy dependent. This is important when analyzing the continuum part of the spectra with no clear and outstanding features. Since the quality of the spectra varied from one proton energy to another, the parameters of the response functions had to be adjusted for each spectrum. The details of this part of the data analysis are given in Ref. [2].

The continuous spectrum above the separation energy dividing the bound and unbound region shows an approximately linear shape up to a well-defined excitation energy E_{xE}. Above this excitation energy or, equivalently, below the γ-ray energy given by

$$E_{\gamma E} = E_p - E_{xE}, \tag{1}$$

the spectrum rises abruptly as an exponential curve. The spectrum exhibiting this feature is shown in Fig. 2. The increasing part of the spectrum represents an intense γ-ray production from protons stopping in the target holder and surrounding materials. We treat it as background that exponentially increases with excitation energy and extrapolate it to the region we analyze. For spectra obtained with 15.7 and 16.9 MeV protons, the effect of this extrapolation is negligible. However, for the spectrum with the proton energy of 14.8 MeV, this contribution is already quite important. We therefore did not include spectra measured at proton energies below 14.8 MeV in our analysis since the contribution of the background is essential there.

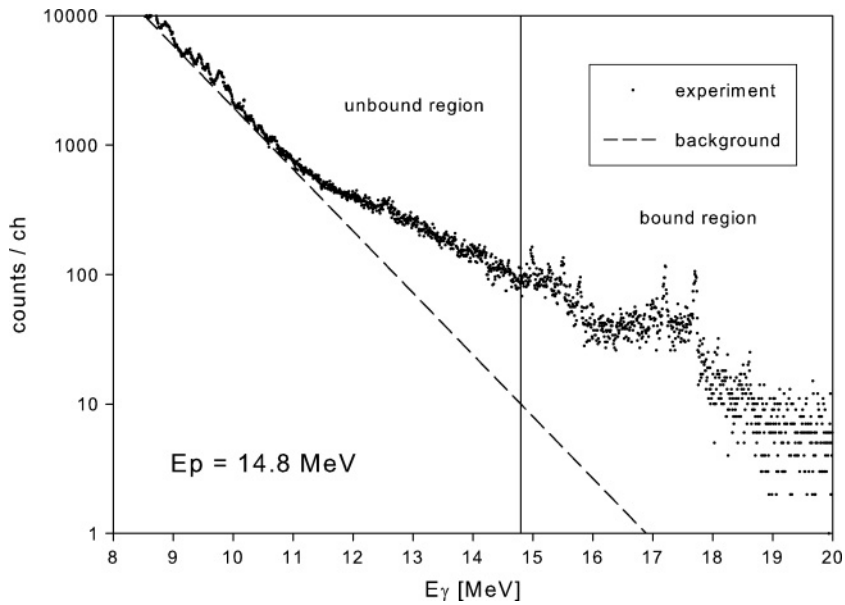

FIG. 2. Low energy background of the 14.8 MeV spectrum, fitted with an exponential curve.

III. ANALYSIS OF THE SPECTRA AND DISCUSSION

Armed with sufficiently accurate response functions, we can confront the statistical and DSD calculations with experimental spectra. The details of the extended DSD formalism are given in [4]; here we give only the expression for the main part of the cross section, namely, the one corresponding to capture to virtual single-particle unbound states, which subsequently decay into the compound nucleus. The measure of the decay spreading width can be deduced, according to the extended DSD theory, from the imaginary part of the final state optical potential. The expression in the notation of [4] is given by

$$\frac{d^2\sigma}{dE_\gamma d\Omega_\gamma} = \frac{1}{j_{\rm inc}}\frac{2}{\hbar}\frac{E_\gamma^2}{(\hbar c)^3}\int d^3\mathbf{r}(-W(r))|\langle\mathbf{r}|G^+H_\gamma|\psi^+\rangle|^2, \tag{2}$$

where G^+ is the outgoing wave Green's function of the optical model Hamiltonian with real and imaginary part

$$H_{\rm opt} = H_{\rm re} + iW(r), \tag{3}$$

appropriate for modeling the single-particle captured state of the proton. $|\psi^+\rangle$ is the energy averaged initial state of the system with a coherent mixture of the incoming proton with energy E_p in the complex initial potential (responsible for the direct process) and the final nucleus in the giant resonance state. This initial system decays by emitting the γ ray via one-body electromagnetic interaction, denoted by H_γ. The energy of the outgoing photon is denoted by E_γ and the density of the initial proton flux by $j_{\rm inc}$.

We would like to remind the reader that in direct reaction models, it is assumed that in the first stage of the reaction the incoming nucleon excites simple configurations of the target nucleus. More complex configurations are excited in

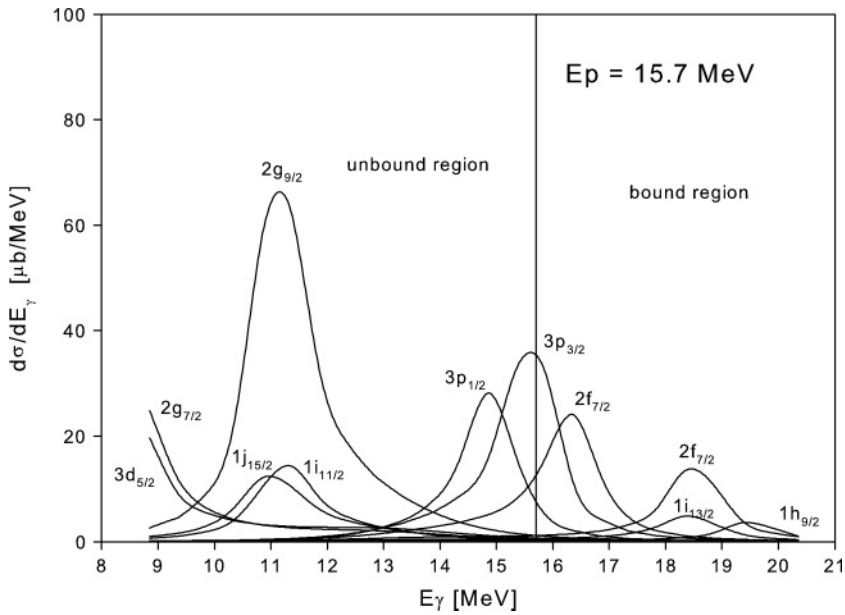

FIG. 3. Extended DSD calculation with the reduced imaginary potential used to generate Green's function G^+. Real potential depth was set at 60.87 MeV to reproduce well-defined bound single-particle states in ^{209}Bi.

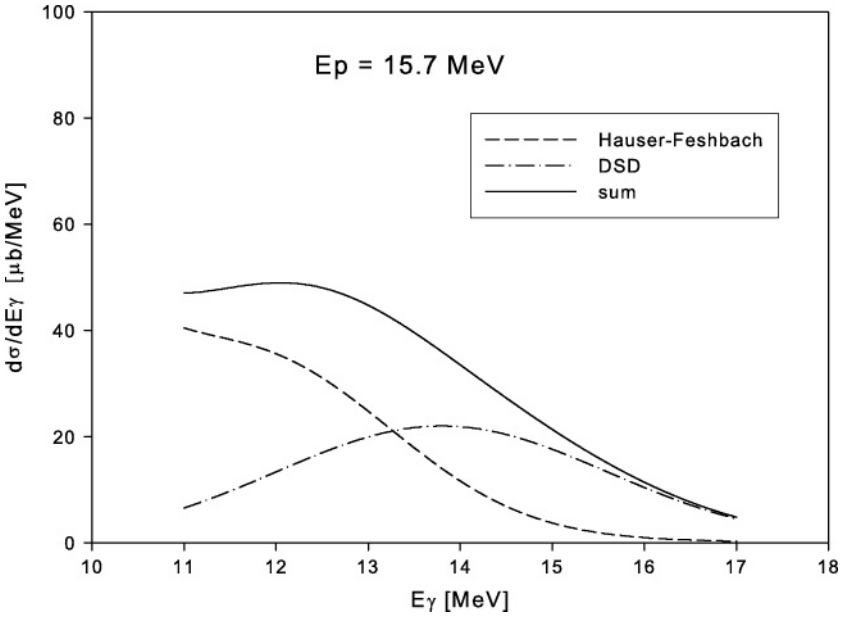

FIG. 4. Extended DSD calculation with statistical cross section obtained with the standard Hauser-Feshbach calculation using the GNASH-FKK code.

later stages of the process. Here, we are explicitly interested in the first stage of the reaction, which involves excitation of the target nucleus to the giant dipole resonance. In Feshbach's [10,11] projection-operator formalism, the exact initial state $|\psi^+\rangle$ is therefore divided into the elastic channel state P, the doorway state D, and the rest of the states Q, such that

$$|\psi^+\rangle = (P + D + Q)|\psi^+\rangle. \tag{4}$$

The projection operators P, D, and Q satisfy the relations $P + D + Q = 1$ and $P^2 = P$, $D^2 = D$, and $Q^2 = Q$. The role of the doorway state D is played in the DSD model by the giant dipole resonance. Although the Q states are eliminated explicitly from the formalism, they have an indirect role in generating the damping width of the giant resonance and the complex nature of the coupling form factor [12,13]. The details of the procedure leading to the final form of the transition amplitude and cross section can be found in [14].

With the expression given in Eq. (2), one treats the DSD process in much the same way as the capture to a bound final state. The spreading of the single-particle strength of the particular bound final state in the DSD calculation is taken into account through spectroscopic factors. In the expression above, the spreading is continuous and dictated by the final state optical potential. In the limit $W \to 0$, the cross sections integrated over the energy obtained from Eq. (2) indeed coincide with the usual DSD expressions. Proper treatment of the DSD process requires complex correction factors for direct and semidirect terms, resulting from the use of different sets of potential parameters in the initial and final single-particle wave functions. Those factors remedy the violation of charge conservation implied by such a treatment. In [14], the correction

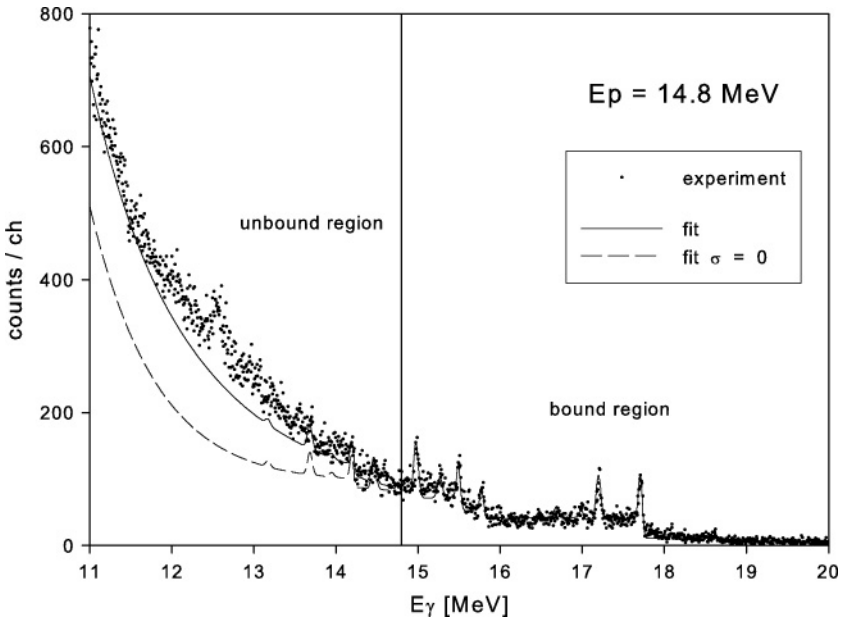

FIG. 5. Fit (solid line) to the γ-ray spectrum (dots), using the cross section very close to that in Fig. 3 and folded with the response function. Fit sensitivity is illustrated by plotting the curve with the cross section set to zero (dashed line). Proton energy was 14.8 MeV.

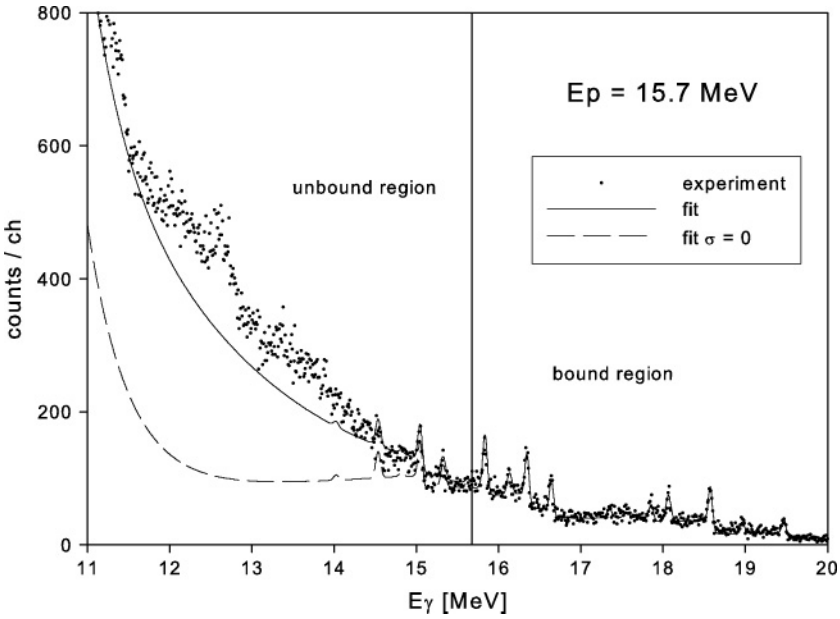

FIG. 6. Same as Fig. 5, but for 15.7 MeV.

factors were introduced. Subsequently, it was demonstrated that by their usage a consistent description of the available data with DSD theory can be achieved throughout the nuclear chart (see [15] and references therein). We, therefore, included our factors in Eq. (2) when treating $(P + D + Q)|\psi^+\rangle$ and did not use the approach suggested in [4], which adds an empirical imaginary part to the symmetry potential. The real form factor is based on the Steinwedel-Jensen hydrodynamic model of the giant dipole state with a symmetry potential strength of $V_1 = 135$ MeV, which proves to be universally valid for the entire mass range of measured data and is adequate for both neutron and proton capture. Recalculation of the results presented in [4] for the 19.6 MeV proton capture, however, shows an almost identical result from both approaches in this specific case. On the other hand, our approach is much more consistent when treating capture to the bound states in ^{209}Bi. In particular, for the high spin state $1i_{13/2}$, the discrepancy between the theory and the experiment has been removed [1].

The extended DSD calculations are presented in Fig. 3 with the reduced imaginary potential generating Green's function in order to show the sequence and relative population of the single-particle strengths. The depth of the real potential was set at 60.87 MeV in order to reproduce the bound single-particle states in ^{209} Bi. It is evident that the $2g_{9/2}$, $1i_{11/2}$, and high spin $1j_{15/2}$ strengths are coincident.

The results of the extended DSD calculation with proper values of the optical potential are given in Fig. 4 together with the statistical cross section obtained with the standard Hauser-Feshbach calculation using our own code STAT and GNASH-FKK [16]. The contribution from the extended DSD mechanism is almost the same for all of the proton energies. The statistical contribution tends to increase in the region of the

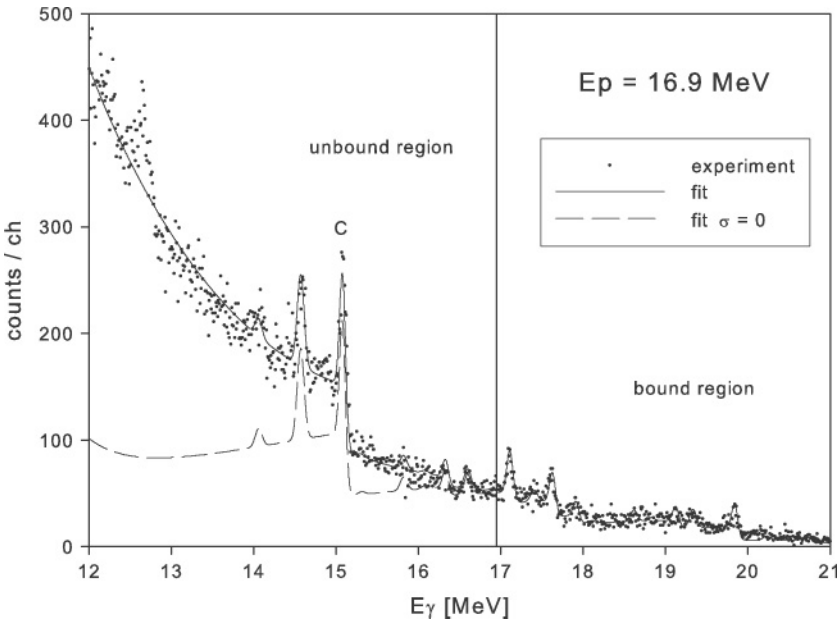

FIG. 7. Same as Fig. 5, but for 16.9 MeV. Large peak C at 15.1 MeV is from the ^{12}C$(p, p'\gamma)$ reaction on the target backing.

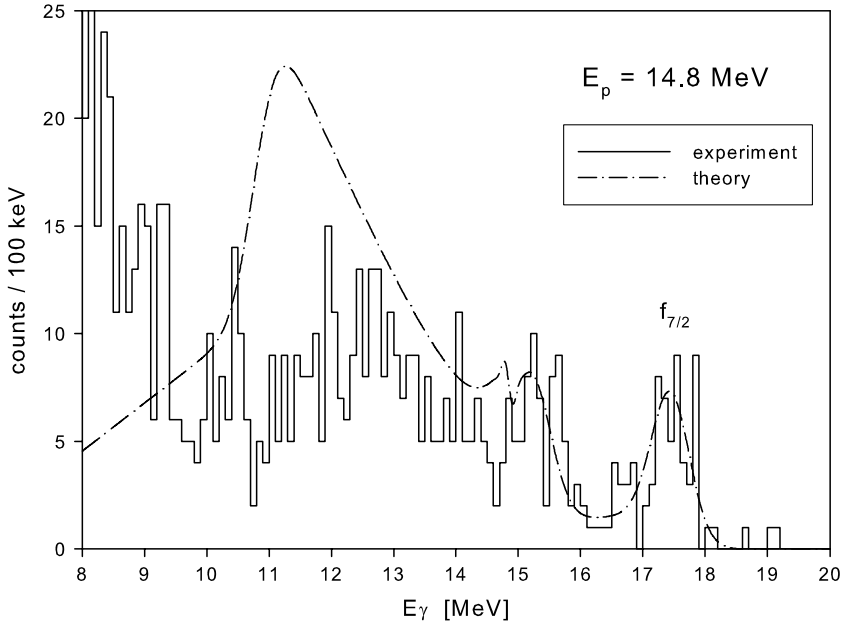

FIG. 8. Normalized coincidence spectra in which the primary γ ray is in coincidence with the low energy photon from the decay of the $2f_{7/2}$ single-particle state. Incident proton energy $E_p = 14.8$ MeV. Curve represents the combined contribution from the extended DSD and statistical processes, assuming all the populated states at the excitation energies with closed neutron channel decay to the $2f_{7/2}$ single-particle state.

giant dipole resonance with increasing proton energy. The $E1\gamma$ transmission coefficients of Kopecky and Uhl [17] were used here. They give results which are almost identical to the ones based on the Brink-Axel hypothesis [18]. The optical model parameters were taken from a recent study [19] and taken to be the same for representing the initial state and the final Green's function calculation. The DSD contribution is dominant only close to the separation line dividing the bound and unbound proton states in ^{209}Bi. Even so, the high resolution spectra are quite sensitive to any, even continuous, contributions close to the separation line in the unbound region. Figures 5–7 show the fits to the spectra due to the cross section given in Fig. 4 folded with the corresponding response functions. The sensitivity of the fit is illustrated by plotting curves with no contribution to the cross section from unbound states. It is evident that the summed statistical and the DSD contribution to the cross section in the unbound region is reasonably well supported by the measured spectra. This is true for all the spectra obtained with different proton energies. However, while the spectrum at the proton energy of 16.9 MeV is almost perfectly reproduced above $E_\gamma = 13$ MeV, the spectra at $E_p = 15.7$ MeV and $E_p = 14.8$ MeV show some additional yield in the region of γ-ray energies between 12 and 14 MeV.

A prominent peak can be seen at $E_\gamma = 12.5$ MeV at all three proton energies. This peak is most likely a doublet of the 12 703 and 12 435 keV γ rays produced in the ^{12}C$(p, p'\gamma)$ and ^{16}O$(p, p'\gamma)$ reactions, respectively [20]. Although the carbon target backing was only 5 μ/cm^2 thick and the targets were freshly made and kept in vacuum when not used, the ground state transitions in both ^{12}C (4438 keV) and ^{16}O (6129 keV)

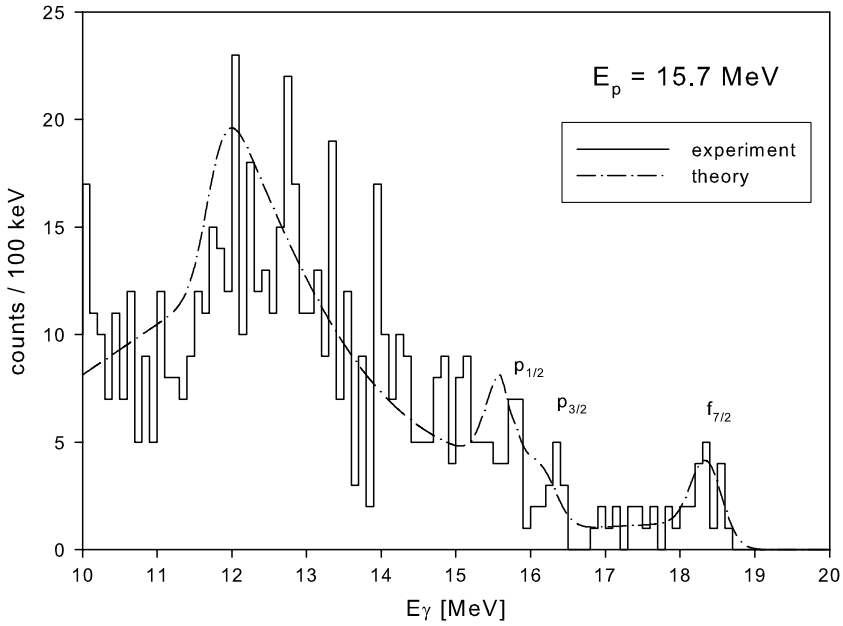

FIG. 9. Same as Fig. 8, but for 15.7 MeV.

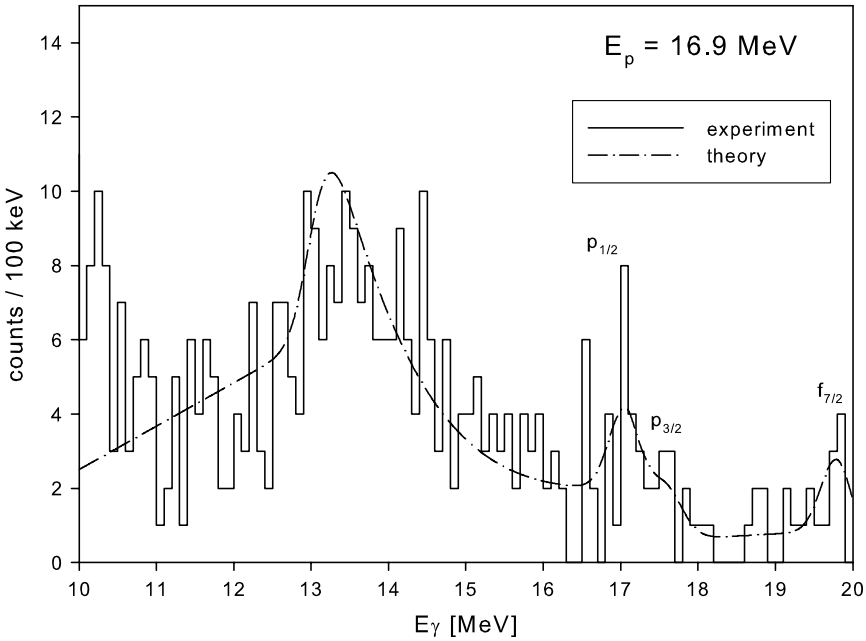

FIG. 10. Same as Fig. 8, but for 16.9 MeV.

produced the highest peaks in our spectra, because of the trigger condition that required high energy γ rays. In addition, the proton beam hitting the Al target frame led to the presence of γ rays from the ^{27}Al$(p, p'\gamma)$ and ^{27}Al$(p, \gamma)^{28}$Si reactions in the low energy part of the spectra. In the latter reaction, many narrow resonances are known at low proton energies [21]. They lead to excited states of ^{28}Si in the excitation energy range between 10 and 15 MeV. Some of these resonances decay by γ-ray emission to the ground state and could possibly cause the increase of the continuous background between 12 and 14 MeV in Figs. 5–7. Apart from this contamination, the energy dependence of the continuous part of the spectra obtained at different proton energies is not prominent and follows the predicted shape quite well. No attempt was made to adjust any of the parameters of the models. The initial and final optical model parameters were taken to be the same since very little information exists about the optical model parameters in the unbound region close to $E_p = 0$. The numerous parameters of the Hauser-Feshbach approach were taken unchanged as compiled in the GNASH-FKK code.

Coincidence spectra for the three proton energies are given in Figs. 8–10. They ensure that in the continuum region one really observes the final nucleus ^{209}Bi. In this spectrum, the primary γ-ray is in coincidence with the 896 keV energy photon from the decay of the $2f_{7/2}$ single-proton state in ^{209}Bi. The continuum states, populated in the capture process, decay by γ-ray emission to lower-lying states. The high spin states decay predominantly to the $1h_{9/2}$ ground state.

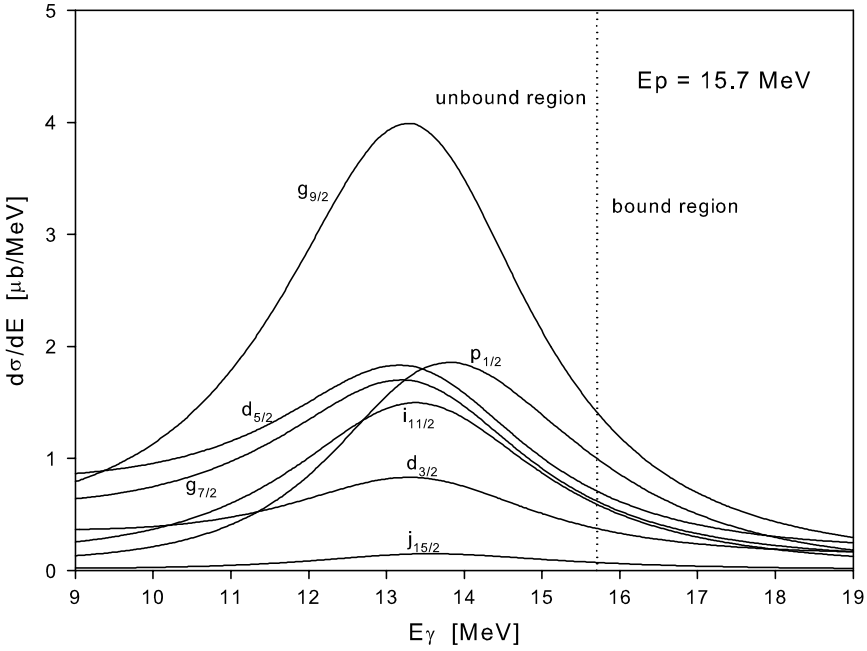

FIG. 11. Relative contribution to the cross section from different angular momentum components as predicted by the extended DSD model. For clarity, only the components which are predominantly unbound are shown.

The dipole decay of states with the $2g_{9/2}$ single-particle strength to the $2f_{7/2}$ state is strongly enhanced by favorable angular momentum and spin factors [22] compared to the decay to the ground state. The coincidence spectra close to the separation line, therefore, reflect the extended DSD contribution from $2g_{9/2}$ strength and all of the contributions from the lower-l states in the unbound region. The former cannot decay to the high spin ground state of the final nucleus. At the excitation energy where the neutron decay channel is opened, the coincidence cross section decreases rapidly. This is evident from the measured spectra which reveal broad peaks caused by a sudden drop in the yield above the excitation energy of 7.46 MeV, which corresponds to the neutron separation energy of the final nucleus. The curves obtained using the cross sections from the extended DSD and statistical processes, given in Fig. 4, are in fair agreement with the experimental data. We made no attempt to reduce and so adjust the absolute values of the cross sections to the experimental spectra. The curves shown are significantly above the experimental points, indicating that the branching ratio for decay to the $2f_{7/2}$ state is roughly 70% in the 4 MeV wide interval above the separation line. This is in agreement with the extended DSD calculations in which the transitions to the high spin states $h_{9/2,11/2}$, $i_{11/2}$, and $j_{13/2,15/2}$ and partly the states $f_{5/2,7/2}$, which directly decay to the ground state, were omitted. The contributions to the cross section from different single-particle configurations concentrated in the unbound region are shown in Fig. 11. The extended DSD approach could be tested thoroughly using higher proton energies to avoid significant statistical contribution to the cross section. However, the calculation at higher proton energy, say at 20 MeV, indicates that the cross section for populating the states close to the separation line is indeed predominantly of the DSD character, but rather small and difficult to measure. The medium-mass nuclei are better suited for such a test, as pointed out in [4].

IV. CONCLUSION

High resolution spectra from fast proton capture in ^{208}Pb were collected and analyzed in the region of radiative capture to unbound states. The ungated γ-ray spectra were adequately reproduced by a combination of the statistical and the extended DSD contribution. The latter dominates only in the region close to the separation line dividing the bound and unbound states in ^{209}Bi. The coincidence spectra reveal a broad structure, which is consistent with a prediction that combined extended DSD and statistical contributions. At high enough excitation energies of the final nucleus, the coincidence spectrum shows no yield. The nucleus then decays through the open neutron channel so the coincidence signal from decay of the $2f_{7/2}$ state is lost. No other discrete features in the unbound region were found, despite the pronounced electrostatic potential barrier preventing the proton and α-particle decay. The only exception is the discrete $3p_{1/2}$ fragment just above the separation line. The distribution of high spin $1i_{11/2}$ and $1j_{15/2}$ strengths can be deduced from the extended DSD model and are in qualitative agreement with the distributions observed and interpreted in stripping reactions.

[1] M. Lipoglavšek *et al.*, Phys. Lett. **B593**, 61 (2004).
[2] M. Lipoglavšek *et al.*, Nucl. Instrum. Methods A **557**, 523 (2006).
[3] S. Gales, C. P. Massolo, S. Fortier, and J. P. Schapira, Phys. Rev. C **31**, 94 (1985).
[4] W. E. Parker, M. B. Chadwick, F. S. Dietrich, J. E. Kammeraad, S. J. Luke, K. E. Sale, R. M. Chasteler, M. A. Godwin, L. H. Kramer, G. J. Schmid, H. R. Weller, and A. K. Kerman, Phys. Rev. C **52**, 252 (1995).
[5] G. E. Brown, Nucl. Phys. **57**, 339 (1964).
[6] J. F. Sharpey-Schafer, Nucl. Phys. News **14**, 5 (2004).
[7] R. T. Newman *et al.*, Balkan Phys. Lett. Special Issue, 182 (1998).
[8] G. Duchene *et al.*, Nucl. Instrum. Methods **A432**, 90 (1999).
[9] R. Brun, F. Bruyant, M. Maire, A. C. McPherson, P. Zanarini, GEANT3, CERN Data Handling Division, Geneva (1987).
[10] H. Feshbach, *Theoretical Nuclear Physics: Nuclear Reactions*, (Wiley, New York, 1992).
[11] W. L. Wang and C. M. Shakin, Phys. Rev. C **5**, 1898 (1972).
[12] R. Satchler, Phys. Lett. **B35**, 279 (1971).
[13] M. Potokar, Phys. Lett. **B46**, 346 (1973).
[14] A. Likar and T. Vidmar, Nucl. Phys. **A591**, 458 (1995); **A593**, 69 (1995).
[15] A. Likar, T. Vidmar, Nucl. Phys. **A635**, 43 (1998).
[16] Oak Ridge National Laboratory, Radiation Safety Information Computational Center, PSR-125, GNASH-FKK, 2004.
[17] J. Kopecky and M. Uhl, Phys. Rev. C **41**, 1941 (1995).
[18] P. Axel, Phys. Rev. **126**, 671 (1962).
[19] A. J. Koning and J. P. Delaroche, Nucl. Phys. **A713**, 231 (2003).
[20] *Table of Isotopes*, 8th ed., edited by R. B. Firestone and V. S. Shirley (Wiley, New York, 1996).
[21] J. Brenneisen *et al.*, Z. Phys. A **352**, 149 (1995).
[22] A. de Shalit and H. Feshbach, *Theoretical Nuclear Physics: Nuclear Structure* (Wiley, New York, 1990).